Applied Physics B (2023) 129:13
https://doi.org/10.1007/s00340-022-07953-1

Applied Physics B
Lasers and Optics

RESEARCH

Stokes correlation to estimate topological charge from the speckle pattern

Tushar Sarkar[1] · **Rakesh Kumar Singh**[1]

Received: 2 April 2022 / Accepted: 30 November 2022 / Published online: 15 December 2022

Abstract
The orbital angular momentum (OAM) of the vortex or helical beam, connected with the topological charge (TC) of the beam, has been used as an alternative degree of freedom to encode and decode the information in the optical signals. Many detection schemes have been established to determine the TC configurations and decode the information at the receiver end of the encoded information from the transmitter end for the free space. However, when the helical beam is transmitted through the scattering medium, its wavefront is spatially scrambled without any direct information about the incident helical beam. Here, we propose and experimentally demonstrate a new approach to estimate the TC of the helical beam from the non-imaged randomly scattered pattern. The technique utilizes Stokes parameters (SPs) of the random field to evaluate higher-order SPs fluctuation correlation. A complete theoretical model of the technique is presented and verified with numerical simulation and experimental tests. A good agreement is found between the simulation and experimental results.

1 Introduction

A light beam with a spiral phase structure $\exp(im\varphi)$ and orbital angular momentum (OAM) of $m\hbar$(where $\hbar$ is a plank's constant) is referred to as a helical beam [1–4]. Term φ represents the azimuthal coordinates and m denotes the TC of the beam [2, 3]. A helical beam possesses a central dark core in the amplitude distribution and this arises due to a phase singularity in the helical wavefront [3, 4]. The OAM of the helical beam is a crucial parameter and has shown many interesting applications in optical communication, particle trapping, image processing, and optical testing [4–7]. Remarkably, channel strength and spectral efficiency in optical communications are enhanced by OAM encoding and mode multiplexing methods, since OAM modes with various m are theoretically immeasurable and orthogonal to one another in Hilbert space [5]. Hence, to decode the data with various OAM states at the receiver end in OAM communication, a precise estimation of the TC connected with the helical beam is of great indispensable. Till now, a variety of approaches have been established to detect the TC of the helical beam based on interference and diffraction. In the interferometric approach, the interference fringes are recorded to monitor the TC values after a helical beam interferes with a reference beam, such as a plane wave, or spherical wave [8–11]. However, interferometric systems require complicated optical setups and are sensitive to external disturbances. To overcome this issue, a helical beam was diffracted through a specially designed geometric aperture including a triangular aperture [12, 13], annular gratings [14], and a translated single slit [15]. In a recent development, a gradually changing-period spiral spoke grating (GCPSSG) was introduced to monitor the magnitude and sign of the TC of the helical beam. The magnitude of TC was evaluated by enumerating the petal in the diffraction pattern and the sign was distinguished from the rotation of the twisted fringes with respect to the grating [16]. These techniques were implemented in free space.

On the other hand, the existence of a scattering media in the propagation path distorts the wavefront of the incident beam and plays a detrimental role in practical applications [17]. Propagation of the incident coherent beam in the presence of an inhomogeneous media scrambles the wavefront and generates a granular pattern i.e. speckle [18]. The speckle patterns don't have any direct analogize with the beam but the beam information is hidden in this pattern. The information-bearing properties of the speckle patterns were explored to develop different

✉ Rakesh Kumar Singh
krakeshsingh.phy@iitbhu.ac.in

[1] Laboratory of Information Photonics and Optical Metrology, Department of Physics, Indian Institute of Technology (Banaras Hindu University), Varanasi 221005, India

detection schemes for the recovery of incident helical beams. Researchers have used coherent light to generate speckle patterns and utilized information-bearing properties of this pattern to develop detection techniques for the recovery and estimation of TC of the helical beam [19–25] and in the examination of polarization properties [26]. In a recent development, the Hanbury-Brown Twiss effect was combined with off-axis holography to estimate the TC of the helical beam. A distribution of cross-covariance of the random intensity pattern was utilized to estimate the TC by enumerating the number of petals [27]. In addition, some significant detection techniques have been developed in the last decade to detect the TC and spiral phase profile of the helical beam with partially coherent light [28–30]. Recently, incoherent light has also been explored to develop detection schemes for the recovery of TC and spiral phase profile of the helical beam propagating through rough scattering layers [31–33].

In this paper, we propose a new approach to estimate the TC of an incident helical beam from the random light using higher-order Stokes parameters (SPs) correlation. Here we present a new theoretical basis to estimate the TC of the incident helical beam propagating through the scatterer by applying higher-order SPs correlation. To develop a new theoretical basis, SPs of the random light are used and higher-order correlations between SPs fluctuations are evaluated. This provides a 4×4 correlation matrix that contains 16 elements. Out of these 16 elements only one element is considered to build a theoretical basis and subsequently apply for the estimation of the TC of the incident helical beam. To validate the proposed approach, we design a highly stable experimental geometry in a coaxial propagation of two orthogonal polarization states of the light and use this configuration to estimate the TC of the incident helical beam from the random light. A detailed theoretical model, numerical simulation, and experimental results are presented below.

2 Methodology

Let us consider an orthogonally polarized monochromatic light source. The x-polarization state of the beam is loaded with a spiral wavefront and the y-polarization state is a plane wave. These two orthogonal polarization states coaxially travel along the z-direction. The complex amplitude at the $z=0$ plane is expressed as

$$\mathrm{U}(\hat{\boldsymbol{r}}) = U_x(\hat{\boldsymbol{r}})\hat{e}_x + U_y(\hat{\boldsymbol{r}})\hat{e}_y, \tag{1}$$

where $U_x(\hat{\boldsymbol{r}}) = A_m(\hat{\boldsymbol{r}})\exp[im\varphi(\hat{\boldsymbol{r}})]$ and $U_y(\hat{\boldsymbol{r}}) = A_0(\hat{\boldsymbol{r}})$. $\hat{\mathrm{e}}_\mathrm{x}$ and $\hat{\mathrm{e}}_\mathrm{y}$ represent unit vectors along the x and y-polarization direction, respectively, and $\hat{\boldsymbol{r}}$ is the spatial position vector at the source plane. $A_m(\hat{\boldsymbol{r}})$, $A_0(\hat{\boldsymbol{r}})$ indicate the amplitude distributions of the helical beam and non-helical beam. The term $\exp[im\varphi(\hat{\boldsymbol{r}})]$ denotes the azimuthal phase structure over the transverse plane with a phase singularity in the heart of a wavefront.

Now the beam transmits through a random scatterer and is detected at any arbitrary distance z from the source as represented in Fig. 1. The complex field at the detector plane is represented as

$$\mathrm{U}(\boldsymbol{r}) = FR\left[\mathrm{U}(\hat{\boldsymbol{r}})\mathrm{e}^{i\phi(\hat{\boldsymbol{r}})}\right], \tag{2}$$

where $\mathrm{U}(\boldsymbol{r})$ indicates the random field at the detector plane. FR is Fresnel transform to accommodate the propagation effect from the scattering plane to the detector plane located at distance z. $\phi(\hat{\boldsymbol{r}})$ indicates the stochastic phase introduced by the diffuser, $\boldsymbol{r}$ is the transverse spatial position vector at the detector plane. The random field at the detector plane, situated in the Fresnel regime, and given as

$$\mathrm{U}(\boldsymbol{r}) = \int h(\boldsymbol{r},\hat{\boldsymbol{r}})\mathrm{U}(\hat{\boldsymbol{r}})e^{i\phi(\hat{\boldsymbol{r}})}d\hat{\boldsymbol{r}}, \tag{3}$$

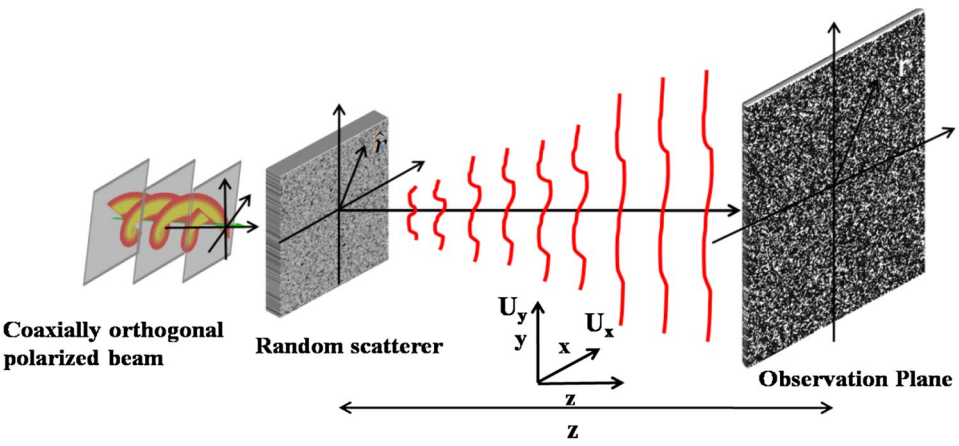

Fig. 1 Schematic representation of the creation of the random electromagnetic field by orthogonally polarized incident light fields

For the free space propagation, the Fresnel Kernel is represented as

$$h(\boldsymbol{r},\hat{\boldsymbol{r}}) = \frac{\exp(ikz)}{i\lambda z}\exp\left(ik\frac{|\hat{\boldsymbol{r}}|^2+|\boldsymbol{r}|^2-2\boldsymbol{r}\cdot\hat{\boldsymbol{r}}}{z}\right), \tag{4}$$

where λ denotes the wavelength of the incident beam and $k=\frac{2\pi}{\lambda}$ represents wave number.

The SPs of the instantaneous random field is expressed as [34, 35]

$$S_p(\boldsymbol{r}) = \sum_{a,b}\sigma_{ab}^{p}U_a^*(\boldsymbol{r})U_b(\boldsymbol{r}), \quad (a,\ b\ =\ x,\ y \text{ and } p\ =\ 0,\ 1,\ 2,\ 3) \tag{5}$$

The 2×2 identity matrix σ^0 and the three Pauli spin matrices are expressed as

$$\sigma^0=\begin{pmatrix}1&0\\0&1\end{pmatrix},\ \sigma^1=\begin{pmatrix}1&0\\0&-1\end{pmatrix},\ \sigma^2=\begin{pmatrix}0&1\\1&0\end{pmatrix},\sigma^3=\begin{pmatrix}0&-i\\i&0\end{pmatrix}, \tag{6}$$

The SPs fluctuations with respect to their average value are expressed as

$$\Delta S_p(\boldsymbol{r}) = S_p(\boldsymbol{r}) - < S_p(\boldsymbol{r}) >, \tag{7}$$

where $S_p(r)$ is the SP at a special spatial point and $<S_p(r)>$ indicates its average value. The statistical features of the random light are characterized by correlations between the SPs fluctuations. All presumable pairs of the two-point SPs correlation are described by a 4×4 matrix $C_{pq}(\boldsymbol{r}_1,\boldsymbol{r}_2)$ with elements

$$\begin{aligned}C_{pq}(\boldsymbol{r}_1,\boldsymbol{r}_2) &= \langle\Delta S_p(\boldsymbol{r}_1)\Delta S_q(\boldsymbol{r}_2)\rangle\\ &= \langle S_p(\boldsymbol{r}_1)S_q(\boldsymbol{r}_2)\rangle - \langle S_p(\boldsymbol{r}_1)\rangle\langle S_q(\boldsymbol{r}_2)\rangle\\ &= \sum_{a,b}\sum_{c,d}\sigma_{ab}^{p}\sigma_{cd}^{q}\langle U_a^*(\boldsymbol{r}_1)U_b(\boldsymbol{r}_1)U_c^*(\boldsymbol{r}_2)U_d(\boldsymbol{r}_2)\rangle\\ &\quad-\sum_{a,b}\sigma_{ab}^{p}\langle U_a^*(\boldsymbol{r}_1)U_b(\boldsymbol{r}_1)\rangle\sum_{c,d}\sigma_{cd}^{q}\langle U_c^*(\boldsymbol{r}_2)U_d(\boldsymbol{r}_2)\rangle,\end{aligned} \tag{8}$$

where parenthesis $\langle.\rangle$ indicates the ensemble average. The 4th-order correlation can be explained in terms of the 2nd-order correlation of the Gaussian random field. Therefore the correlation matrix $C_{pq}(\boldsymbol{r}_1,\boldsymbol{r}_2)$ is represented as

$$\begin{aligned}C_{pq}(\boldsymbol{r}_1,\boldsymbol{r}_2) &= \sum_{a,b}\sum_{c,d}\sigma_{ab}^{p}\sigma_{cd}^{q}\left[\langle U_a^*(\boldsymbol{r}_1)U_b(\boldsymbol{r}_1)\rangle\langle U_c^*(\boldsymbol{r}_2)U_d(\boldsymbol{r}_2)\rangle+\langle U_a^*(\boldsymbol{r}_1)U_d(\boldsymbol{r}_2)\rangle\langle U_c^*(\boldsymbol{r}_2)\ U_b(\boldsymbol{r}_1)\rangle\right]\\ &\quad-\sum_{a,b}\sum_{c,d}\sigma_{ab}^{p}\sigma_{cd}^{q}\langle U_a^*(\boldsymbol{r}_1)U_b(\boldsymbol{r}_1)\rangle\langle U_c^*(\boldsymbol{r}_2)U_d(\boldsymbol{r}_2)\rangle\end{aligned} \tag{9}$$

$$= \sum_{a,b}\sum_{c,d}\sigma_{ab}^{p}\sigma_{cd}^{q}W_{ad}(\boldsymbol{r}_1,\boldsymbol{r}_2)W_{bc}^*(\boldsymbol{r}_1,\boldsymbol{r}_2), \tag{10}$$

where $W_{ad}(\boldsymbol{r}_1,\boldsymbol{r}_2) =< U_a^*(\boldsymbol{r}_1)U_d(\boldsymbol{r}_2) >$ are the elements of the 2×2 coherence-polarization (CP) matrix which characterizes the vectorial stochastic field [35, 36]

$$W(\boldsymbol{r}_1,\boldsymbol{r}_2)=\begin{pmatrix}W_{xx}(\boldsymbol{r}_1,\boldsymbol{r}_2)&W_{xy}(\boldsymbol{r}_1,\boldsymbol{r}_2)\\W_{yx}(\boldsymbol{r}_1,\boldsymbol{r}_2)&W_{yy}(\boldsymbol{r}_1,\boldsymbol{r}_2)\end{pmatrix} \tag{11}$$

Therefore, all pairs of SPs fluctuations correlation are represented as [22, 34]

$$C_{pq}(\boldsymbol{r}_1,\boldsymbol{r}_2) = \begin{Bmatrix}C_{00}(\boldsymbol{r}_1,\boldsymbol{r}_2)&C_{01}(\boldsymbol{r}_1,\boldsymbol{r}_2)&C_{02}(\boldsymbol{r}_1,\boldsymbol{r}_2)&C_{03}(\boldsymbol{r}_1,\boldsymbol{r}_2)\\C_{10}(\boldsymbol{r}_1,\boldsymbol{r}_2)&C_{11}(\boldsymbol{r}_1,\boldsymbol{r}_2)&C_{12}(\boldsymbol{r}_1,\boldsymbol{r}_2)&C_{13}(\boldsymbol{r}_1,\boldsymbol{r}_2)\\C_{20}(\boldsymbol{r}_1,\boldsymbol{r}_2)&C_{21}(\boldsymbol{r}_1,\boldsymbol{r}_2)&C_{22}(\boldsymbol{r}_1,\boldsymbol{r}_2)&C_{23}(\boldsymbol{r}_1,\boldsymbol{r}_2)\\C_{30}(\boldsymbol{r}_1,\boldsymbol{r}_2)&C_{31}(\boldsymbol{r}_1,\boldsymbol{r}_2)&C_{32}(\boldsymbol{r}_1,\boldsymbol{r}_2)&C_{33}(\boldsymbol{r}_1,\boldsymbol{r}_2)\end{Bmatrix}, \tag{12}$$

The element $C_{23}(\boldsymbol{r}_1,\boldsymbol{r}_2)$ of the matrix is evaluated using Eq. (10)

$$C_{23}(\boldsymbol{r}_1,\boldsymbol{r}_2) = \sum_{a,b}\sum_{c,d}\sigma_{ab}^{2}\sigma_{cd}^{3}W_{ad}(\boldsymbol{r}_1,\boldsymbol{r}_2)W_{bc}^*(\boldsymbol{r}_1,\boldsymbol{r}_2).$$

$$\propto \mathrm{Im}[W_{xy}(\boldsymbol{r}_1,\boldsymbol{r}_2)W_{yx}^*(\boldsymbol{r}_1,\boldsymbol{r}_2)+W_{xx}^*(\boldsymbol{r}_1,\boldsymbol{r}_2)W_{yy}(\boldsymbol{r}_1,\boldsymbol{r}_2)].$$

$$\propto \mathrm{Im}[A+B], \tag{13}$$

where $A=W_{xy}(\boldsymbol{r}_1,\boldsymbol{r}_2)W_{yx}^*(\boldsymbol{r}_1,\boldsymbol{r}_2)$, and $B=W_{xx}^*(\boldsymbol{r}_1,\boldsymbol{r}_2)W_{yy}(\boldsymbol{r}_1,\boldsymbol{r}_2)$.

Let us explore the use of Eq. (13) in the estimation of the TC from the speckle pattern.

$$A = W_{xy}(\boldsymbol{r}_1,\boldsymbol{r}_2)W_{yx}^*(\boldsymbol{r}_1,\boldsymbol{r}_2) = \left\langle U_x^*(\boldsymbol{r}_1)U_y(\boldsymbol{r}_2)\right\rangle\left\langle[U_y^*(\boldsymbol{r}_1)U_x(\boldsymbol{r}_2)]^*\right\rangle, \tag{14}$$

Substituting Eq. (3) into the SPs correlation results in the cancelation of the phase term outside the Fresnel propagation kernel as shown in Eq. (3) and hence this phase term is ignored in Eq. (15) [37]. The spatial stationarity is achieved at an arbitrary z and this allows to replace the ensemble averaging by spatial averaging [36, 37]. Considering $\boldsymbol{r_1}=\boldsymbol{r}+\Delta r$ and $\boldsymbol{r_2}=\boldsymbol{r}$, the cross-covariance of the SPs at the detector

plane is expressed in terms of a two-point correlation function as explained in Eq. (13) and the two-point correlation function is expressed [22, 37] as

$$W_{ab}(\boldsymbol{r}+\Delta\boldsymbol{r},\boldsymbol{r}) = \frac{1}{\lambda^2 z^2}\int\int\int \exp\left(\frac{ik}{2z}[|\hat{\boldsymbol{r}}_2|^2-|\hat{\boldsymbol{r}}_1|^2]\right) \exp\left(\frac{-ik}{z}(\hat{\boldsymbol{r}}_2-\hat{\boldsymbol{r}}_1)\cdot\boldsymbol{r}\right) \exp\left(\frac{-ik\Delta\boldsymbol{r}.\hat{\boldsymbol{r}}}{z}\right)U_a^*(\hat{\boldsymbol{r}}_1) U_b(\hat{\boldsymbol{r}}_2)\mathrm{d}\hat{\boldsymbol{r}}_1\mathrm{d}\hat{\boldsymbol{r}}_2\mathrm{d}\boldsymbol{r}, \tag{15}$$

Using the relation $\int \exp\left(-\frac{ik}{z}(\hat{\boldsymbol{r}}_2-\hat{\boldsymbol{r}}_1)\cdot\boldsymbol{r}\right)\mathrm{d}\boldsymbol{r} = \delta(\hat{\boldsymbol{r}}_2-\hat{\boldsymbol{r}}_1)$. Therefore Eq. (15) modifies to

$$W_{ab}(\Delta\boldsymbol{r}) \propto \int U_a^*(\hat{\boldsymbol{r}})U_b(\hat{\boldsymbol{r}})\exp\left(-\frac{ik\Delta\boldsymbol{r}.\hat{\boldsymbol{r}}}{z}\right)d\hat{\boldsymbol{r}}, \quad (a,\, b = x,\, y) \tag{16}$$

We consider $U_x(\hat{\boldsymbol{r}}) = \mathrm{cir}\left(\frac{\hat{r}}{a}\right)\exp(\mathrm{im}\varphi)$, where a is the radius of a circular aperture and $U_y(\hat{\boldsymbol{r}}) = 1$. Therefore Eq. (16) transforms [38] to

$$W_{xy}(\Delta\boldsymbol{r}) \propto \frac{J_1(2\pi a\Delta\boldsymbol{r}/\lambda z)}{2\pi a\Delta\boldsymbol{r}/\lambda z}\exp(-\mathrm{im}\Delta\varphi), \tag{17}$$

where J_1 represents the Bessel function. Similarly $W_{yx}^*(\Delta\boldsymbol{r}) \propto \frac{J_1(2\pi a\Delta\boldsymbol{r}/\lambda z)}{2\pi a\Delta\boldsymbol{r}/\lambda z}\exp(-\mathrm{im}\Delta\varphi)$, $W_{xx}^*(\Delta\boldsymbol{r}) \propto \frac{J_1(2\pi a\Delta\boldsymbol{r}/\lambda z)}{2\pi a\Delta\boldsymbol{r}/\lambda z}$, and $W_{yy}(\Delta\boldsymbol{r}) \propto 1$.

Substituting the value of $W_{xy}(\Delta\boldsymbol{r}), W_{yx}^*(\Delta\boldsymbol{r}), W_{xx}^*(\Delta\boldsymbol{r})$, and $W_{yy}(\Delta\boldsymbol{r})$, into Eq. (13) Therefore Eq. (13) modifies as

$$C_{23}(\Delta\boldsymbol{r}) \propto \mathrm{Im}\left[\left(\frac{J_1(2\pi a\Delta\boldsymbol{r}/\lambda z)}{2\pi a\Delta\boldsymbol{r}/\lambda z}\exp(-\mathrm{im}\Delta\varphi)\right)^2 + \frac{J_1(2\pi a\Delta\boldsymbol{r}/\lambda z)}{2\pi a\Delta\boldsymbol{r}/\lambda z}\right], \tag{18}$$

Equation (18) connects the source and Stokes correlation function at the detector plane and the distribution of cross-covariance helps to make a relation between topological charge and petals to estimate TC. The SPs correlations are now represented by the function of the difference between the spatial coordinates i.e. $\Delta\mathbf{r}$. The distribution of the coherence function forms petals due to the imaginary part $\mathrm{Sin}2(\Delta\varphi)$ of the cross-covariance function $C_{23}(\Delta\boldsymbol{r})$. Equation (18) is capable to provide an estimation of the TC of an incident helical beam from the randomly scattered light.

This empirical relation is represented as

$$n = 4m, \quad (m,\, n\, =\, 0,\, 1,\, 2,\, 3, \ldots), \tag{19}$$

where m represents topological charge and n denotes petals.

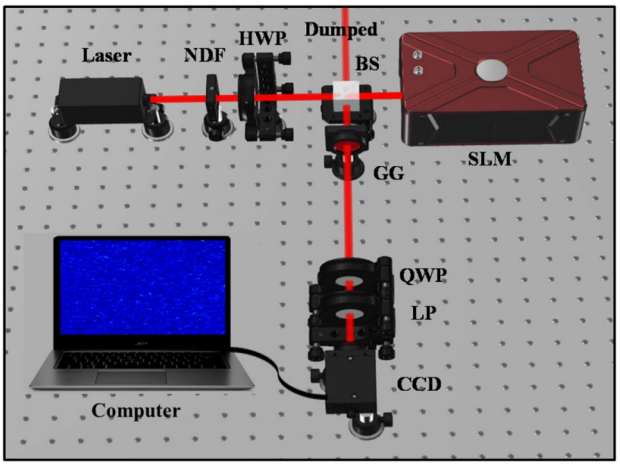

Fig. 2 An experimental setup to estimate the TC of the vortex beam from the speckle pattern. *NDF* neutral density filter, *HWP* half-wave plate, *BS* beam splitter, *SLM* spatial light modulator, *GG* ground glass, *QWP* quarter-wave plate, *LP* linear polarizer, *CCD* charge-coupled device. The dumped beam is not used in the experiment

3 Experiment

To validate the applicability of the proposed method, we design a non-interferometric experimental geometry to estimate the TC of the helical beam as shown in Fig. 2. A spatially filtered x-polarized He–Ne laser light with a wavelength of 632.8 nm is attenuated by a neutral density filter (NDF). The half-wave plate (HWP) at 22.5° is used to orient the input polarization of the incident beam into a diagonal polarization. A 50:50 beam splitter (BS) is inserted to divide the beam into two equal-intensity beams. A transmitted beam from the BS illuminates a phase-only reflective type spatial light modulator (SLM) with a pixel pitch of 8 µm and a resolution of 1920 × 1080 (Pluto from Holoeye). The SLM only allows to modulate the x-polarization state of the incident beam and the y-polarization state of the beam remains un-effected. The SLM is loaded with a computer-generated hologram to generate a helical beam in the x-polarization state. The y-polarization state contains a plane wave. These coaxially propagating beams propagate through the random diffuser (GG) and random scattering from the GG generates a polarization speckle, i.e. speckle with spatial polarization fluctuation [39]. The polarization speckle is analyzed through a quarter-wave plate (QWP) and a linear polarizer (LP). The combination of QWP and LP is used to measure the SPs of the scattered light. The intensity patterns $I(\theta_q, \theta_p)$ are captured by the charged coupled device CCD which is placed at 250 mm from the GG plane for four different combinations of QWP's fast and LP's pass axis orientation (θ_q, θ_p) with respect to the x-axis. The two SPs are measured from the captured intensity speckle patterns by considering the following equations [22].

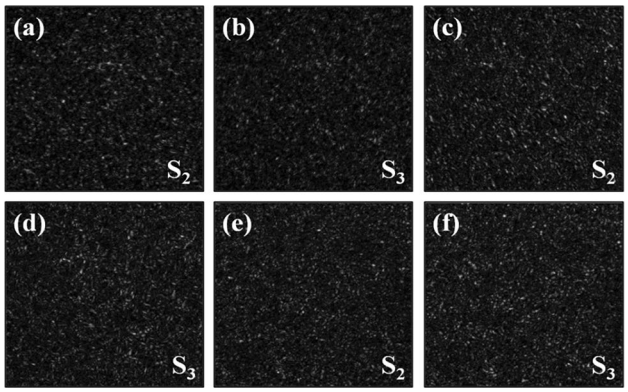

Fig. 3 denotes experimentally measured SPs from the recorded intensity speckle patterns. **a** and **b**, **c** and **d**, **e** and **f** show SPs of the vortex with $m = 1, 2, 3$, respectively

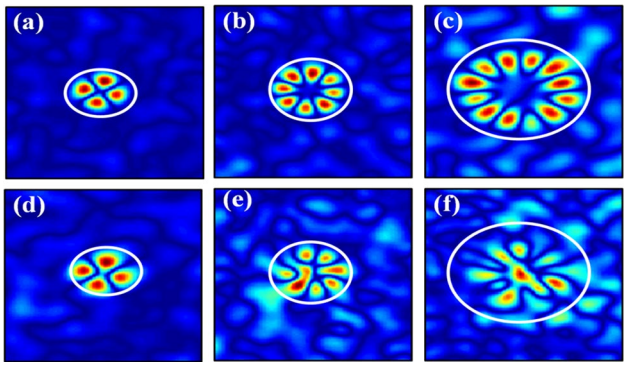

Fig. 4 **a**–**c** represent simulation results for the distribution of coherence function for vortex with $m = 1, 2, 3$, respectively. **d**–**f** are the corresponding experimental results

$$S_2(r) = I(45°, 45°) - I(135°, 135°),$$
$$S_3(r) = I(0°, 45°) - I(0°, 135°), \tag{20}$$

The experimentally measured SPs are used to evaluate the correlation between SPs fluctuation using Eq. (8) and ensemble averaging is replaced by spatial averaging. This process is applied to evaluate cross-covariance $C_{23}(\Delta \boldsymbol{r})$ from the experimentally detected SPs as described in Eq. (18). Finally, the topological charge is estimated by counting petals as described in Eq. (19).

4 Results and discussions

The SPs are measured from the experimentally captured intensity speckle pattern for the helical beams with $m = 1$, 2, 3, and the results are represented in Fig. 3. Figure 3a and b denote recorded SPs (S_2, S_3) from the random intensity pattern for vortex with $m = 1$. Figure 3c and d show SPs (S_2, S_3) for vortex with $m = 2$ and Fig. 3e–f denote SPs (S_2, S_3) for vortex with $m = 3$, respectively. Simulation and experimental results of the distribution of cross-covariance are represented in Fig. 4. Simulation results in Fig. 4a–c represent a distribution of polarization correlation function $C_{23}(\Delta \boldsymbol{r})$ for vortex with $m = 1, 2, 3$, respectively. Corresponding experimental results are represented in Fig. 4d–f. In Fig. 4a, d distribution of coherence function forms 4 petals for vortex with $m = 1$. The distribution of coherence function forms 8 and 12 petals for vortex with $m = 2$ and $m = 3$ are represented in Fig. 4b, e and c, f, , respectively. The complex coherence function of the experimentally detected SPs is examined by considering spatial averaging under the condition of spatial ergodicity at the observation plane. The benefits of spatial averaging had been applied currently in many correlation imaging methods with due importance in spatial statistical optics [40]. This spatial averaging is realized by taking a portion of the SP at the detector plane as a matrix $S_n^{\alpha}(x, y)$ which denotes one realization of the SP of the random field. Here x and y are the pixel spatial coordinates and take values up to 300×300 pixels. The cross-covariance of the SPs for the different realization is indicated as $\sum_{\alpha=1}^{M} \left[\Delta S_m^{\alpha}(x, y) \Delta S_n^{\alpha}(0, 0)\right]/M$. Where, M represents the number of different realizations of the matrix $S_n^{\alpha}(x, y)$ appearing due to pixel-by-pixel movement of the matrix $S_n^{\alpha}(x, y)$ over the experimentally recorded SPs. We have used a random pattern of size 1000×1000 pixels and 2D scanning of $S_n^{\alpha}(x, y)$ over the random pattern gives 700×700 different realizations for averaging. On the other hand, the average value of the Stokes $\langle S_p(\boldsymbol{r}) \rangle$ is obtained by taking the average over the spatial patterns M and represented as $\sum_{\alpha=1}^{M} \frac{[S_m^{\alpha}(x,y)]}{M}$. A small deviation in the experimental results in comparison to the simulation is possibly owing to experimental constraints. Some weak residual modes for corresponding field distribution may appear due to the phase profile used to generate vortex using pixilated SLM [41]. On the other hand, limited size polarization optics in the experiment and background coherence $W_{xx}^{*}(\Delta \boldsymbol{r})$, and $W_{yy}(\Delta \boldsymbol{r})$ in the Eq. (13) also affects the reconstruction quality.

5 Conclusions

We have proposed and experimentally demonstrated a new approach to estimating the TC of the helical beam propagating through the scattering medium. The SPs of the random light are utilized to evaluate the higher-order SPs fluctuation correlation and subsequently applied for the efficient estimation of the incident helical beam. The distribution of the cross-covariance renders the information of the TC of the helical beam. The feasibility of the proposed approach is evaluated by numerical simulation

and followed by the experimental demonstration for the estimation of TC of the helical beam. The proposed experimental configuration is robust and offers flexibility owing to non-interferometric. The applicability of the developed approach has been experimentally demonstrated to estimate helical beams with $m = 1, 2, 3$.

Acknowledgements T. S. acknowledges the University Grant Commission, India for financial support as Senior Research Fellowship.

Author contributions TS: Conceived the idea, investigation, formal analysis, experiment, data analysis, writing—original draft. RKS: Ideas, formulation of research goals and aims, methodology, validation, experimental design, reviewing and editing, supervision, and funding acquisition.

Funding This work is supported by the Council of Scientific and Industrial Research (CSIR), India- Grant No 80 (0092) /20/ EMR-II, Science and Engineering Research Board (SERB) India-CORE/2019/000026, Board of Research in Nuclear Sciences (BRNS) India-58/14/04/2021-BRNS/37092.

Data availability Data underlying the results presented in this paper is not publicly available at this time but may be obtained from the authors upon reasonable request.

Declarations

Conflict of interest The authors declare no conflicts of interest.

References

1. L. Allen, S. Barnett, M.J. Padgett, *Orbital Angular Momentum* (CRC Press, Boca Raton, 2016)
2. A.E. Willner, H. Huang, Y. Yan, Y. Ren, N. Ahmed, G. Xie, C. Bao, L. Li, Y. Cao, Z. Zhao, J. Wang, M.P.J. Lavery, M. Tur, S. Ramachandran, A.F. Molisch, N. Ashrafi, S. Ashrafi, Optical communication using orbital angular momentum beams. Adv. Opt. Photon. **7**(15), 66 (2015)
3. J.P. Torres, L. Torner, *Twisted Photons, Application of Light with Orbital Angular Momentum* (Wiley-VCH, Weinheim, 2011)
4. Y. Shen, X. Wang, Z. Xie, C. Min, X. Fu, Q. Liu, M. Gong, X. Yuan, Optical vortices 30 years on: OAM manipulation from topological charge to multiple singularities. Light Sci. Appl. **8**(19), 90 (2019)
5. J. Wang, Advances in communications using optical vortices. Photon. Res. **4**(16), B14 (2016)
6. M. Kumar, J. Joseph, P. Senthilkumaran, Selective edge enhancement using anisotropic vortex filter. Appl. Opt. **50**(11), 5279 (2011)
7. P. Senthilkumaran, Optical phase singularities in detection of laser beam collimation. Appl. Opt. **42**(3), 6314 (2003)
8. J. Leach, J. Courtial, K. Skeldon, S.M. Barnett, S. Frank-Arnold, M.J. Padgett, interferometric method to measure orbital and spin, or the total orbital angular momentum of a single photon. Phys. Rev. Lett. **92**(4), 013601 (2004)
9. H.I. Sztul, R.R. Alfano, Double-slit interference with Laguerre-Gaussian beams. Opt. Lett. **31**(6), 999–1001 (2006)
10. B. Khajavi, J.R.G. Ureta, E.J. Galvez, Determining vortex-beam superposition by shear interferometry. Photonics **5**(18), 16 (2018)
11. D.P. Ghai, S. Vyas, P. Senthilkumaran, R.S. Sirohi, Detection of phase singularity using a lateral shear interferometer. Opt. Laser Eng. **46**(8), 419 (2008)
12. L. Araujo, M.E. Anderson, Measuring vortex charge with a triangular aperture. Opt. Lett. **36**(11), 787 (2011)
13. L.A. Melo, A.J. Jesus-Silva, W.C. Soares, Direct measurement of the topological charge in elliptical beams using diffraction by a triangular aperture. Sci. Rep. **8**(18), 6370 (2018)
14. S. Zheng, J. Wang, measuring orbital angular momentum (OAM) states of vortex beams with annular gratings. Sci. Rep. **7**(17), 40781 (2017)
15. J. Princeton, C. Narag, N. Hermosa, Probing higher angular momentum of Laguerre–Gaussian beams vis translated single slit. Phys. Rev. Appl. **11**(19), 054025 (2019)
16. Y. Li, Y. Han, Z. Cui, measuring topological charge of vortex beam with gradually changing-period spiral spoke gratting. IEEE Photon. Technol. Lett. **32**(20), 101 (2019)
17. G. Gbur, R.K. Tyson, Vortex beam propagation through atmospheric turbulence and topological charge conservation. J. Opt. Soc. Am. **25**(8), 225 (2008)
18 J.W. Goodman, *Speckle Phenomena in Optics: Theory and Applications* (Roberts-Company, Santa Monica, 2006)
19. C.H. Acevedo, J.R.G. Sepulveda, A. Dogariu, First-order statistics of the phase in optical vortex speckles. J. Opt. Soc. Am. **37**(20), 584 (2020)
20. G.R. Salla, C. Perumangattu, S. Prabhakar, A. Anwar, R.P. Singh, Recovering the vorticity of a light beam after scattering. Appl. Phys. Lett. **107**(15), 021104 (2015)
21. R.V. Vinu, R.K. Singh, Determining helicity and topological structure of coherent vortex beam from laser speckle. Appl. Phys. Lett. **109**(16), 111108 (2016)
22. T. Sarkar, R. Parvin, M.M. Burndavanam, R.K. Singh, Higher-order Stokes-parameter correlation to restore the twisted wave front propagating through a scattering medium. Phys. Rev. A **104**(21), 013525 (2021)
23. W. Yang, G. Situ, Recovery of the topological charge of a vortex beam propagated through a scattering layer. Appl. Opt. **60**(21), B95 (2021)
24. T. Sarkar, R. Parvin, M.M. Burndavanam, R.K. Singh, Unscrambling OAM mode using digital phase-shifting in the Stokes fluctuations correlation. Opt. Lett. **22**(21), 5546 (2021)
25. T. Sarkar, R. Parvin, M.M. Burndavanam, R.K. Singh, Measuring obscured OAM spectrum using Stokes fluctuations in a non-interferometric approach. Opt Laser Eng **155**, 107065 (2022)
26. G.R. Salla, V. Kumar, Y. Miyamoto, R.P. Singh, Scattering of Poincaré beams: polarization speckles. Opt. Express **25**(17), 19886 (2017)
27. L. Chen, R.K. Singh, A. Dogariu, Z. Chen, J. Pu, Estimation topological charge of propagating vortex from single-shot non-imaged speckle. Chin. Opt. Lett. **19**(21), 022603 (2021)
28. R.K. Singh, A.M. Sharma, P. Senthilkumaran, Vortex array embedded in a partially coherent beam. Opt. Lett. **40**(15), 2751 (2015)
29. P.F. Ding, J. Pu, The cross correlation function of partially coherent vortex beam. Opt. Express **22**(14), 1350 (2014)
30. X. Lu, C. Zhao, Y. Shao, J. Zeng, S. Konijnenberg, X. Zhu, S. Popov, H.P. Urbach, Y. Cai, Phase detection of coherence singularities and determination of topological charge of a partially coherent vortex beam. Appl. Phys. Lett. **114**(19), 201106 (2019)
31. X. Liu, J. Zeng, Y. Cai, Review on vortex beams with low spatial coherence. Adv. Phys. X **4**, 507 (2019)
32. D.O. Bezerra, J.P. Amaral, E.J.S. Fonseca, C.R. Alves, A.J. Jesus-Silva, Sorting of spatially incoherent optical vortex modes. Sci. Rep. **10**(20), 2533 (2020)
33. Y. Huang, R.V. Vinu, Z. Chen, T. Sarkar, R.K. Singh, J. Pu, Recovery and characterization of orbital angular momentum

modes with ghost diffraction holography. Appl. Sci. **11**(21), 12167 (2021)
34. G. Wu, D. Kubel, T.D. Visser, Generalized Hanbury Brown-Twiss effect in partially coherent electromagnetic beams. Phys. Rev. A **99**(19), 033846 (2019)
35. D. Kuebel, T.D. Visser, Generalized Hanbury Brown-Twiss effect for Stokes parameters. JOSA A **36**(19), 362 (2019)
36. R.K. Singh, D.N. Naik, H. Itou, M.M. Burndavanam, Y. Miyamoto, M. Takeda, Vectorial van Cittert–Zernike theorem based on spatial averaging: experimental demonstrations. Opt. Lett. **38**(13), 4809 (2013)
37. R.K. Singh, S. Vyas, Y. Miyamoto, Lensless Fourier transform holography for coherence waves. J. Opt. **19**(17), 115705 (2017)
38. P. Vaity, L. Rusch, Perfect vortex beam: Fourier transformation of a Bessel beam. Opt. Lett. **40**(15), 597 (2015)
39. R.K. Singh, D.N. Naik, H. Itou, Y. Miyamoto, M. Takeda, Characterization of spatial polarization fluctuations in scattered field. J. Opt. **16**(14), 105010 (2014)
40. M. Takeda, W. Wang, D.N. Naik, R.K. Singh, Spatial statistical optics and spatial correlation holography: a review. Opt. Rev. **21**(14), 849 (2014)
41 I. Nape, B. Sephton, Y.W. Huang, A. Vallés, C.W. Qiu, A. Ambrosio, F. Capasso, A. Forbes, Enhancing the modal purity of orbital angular momentum photons. APL Photonics. **5**(20), 070802 (2020)